



Cite this: *Energy Adv.*, 2023,  
2, 1818

Received 26th January 2023,  
Accepted 26th September 2023

DOI: 10.1039/d3ya00048f

rsc.li/energy-advances

## Rear textured p-type high temperature passivating contacts and their implementation in perovskite/silicon tandem cells†

Arnaud Walter,<sup>id</sup>\*<sup>a</sup> Brett A. Kamino,<sup>id</sup><sup>a</sup> Soo-Jin Moon,<sup>a</sup> Patrick Wyss,<sup>a</sup>  
Juan J. Diaz Leon,<sup>a</sup> Christophe Allebé,<sup>a</sup> Antoine Descoedres,<sup>a</sup> Sylvain Nicolay,<sup>‡</sup>  
Christophe Ballif,<sup>ab</sup> Quentin Jeangros<sup>a</sup> and Andrea Ingenito<sup>id</sup>\*<sup>a</sup>

**Silicon solar cells based on high temperature passivating contacts are becoming mainstream in the photovoltaic industry. Here, we developed a high-quality boron-doped poly-silicon hole contact. When combined with a co-processed phosphorus-doped poly-silicon electron contact, high-voltage silicon bottom cells could be demonstrated and included in 28.25%-efficient perovskite/Si tandems. The active area was 4 cm<sup>2</sup> active area and the front electrode was screen-printed.**

With efficiencies recently overcoming the 30% mark with laboratory-scale solar cells,<sup>1–3</sup> perovskite/Si (PK/Si) tandem cells are increasingly considered a credible candidate for high-efficiency commercial PV and the technology starts to be part of the development roadmap of most crystalline Si (c-Si) solar cell manufacturers. However, nearly all of the highest efficiency tandem devices reported to date rely on a Si heterojunction (SHJ) bottom cell.<sup>4–6</sup> At the industrial level, the SHJ technology occupies only a small niche of a market moving from the passivated emitter and rear cell (PERC)<sup>7,8</sup> concept towards the use of the tunnel oxide-passivating contact (TOPCon) technology, which is based on high temperature passivating contacts (HTPC).<sup>8,9</sup> In TOPCon devices, the cells and contacts are processed at higher temperature enabling the use of equipment and processes more similar to the PERC technology, along with lower quality wafers. In view of a future industrial deployment, the demonstration of a PK/Si cell built upon more widely used processes or device architectures is hence needed. Such

tandems have been previously produced using industrially-relevant bottom cells based on the PERC/TOPCon technology or a modified TOPCon with rear localized contacts.<sup>7,10</sup> These devices reached efficiencies of 28.7% and 27.6%, respectively, on a 1 cm<sup>2</sup> active area. However, these designs suffer from limited passivation at the rear of the c-Si cell, and, in the second case, from an increased fabrication complexity. More recently, a tandem cell based on a TOPCon c-Si cell featuring a p-type rear contact deposited on a textured wafer was shown to reach an efficiency of 28.2%, albeit on 0.124 cm<sup>2</sup> and on an n-type wafer.<sup>11</sup> Here, we demonstrate a 4 cm<sup>2</sup> >28%-efficient tandem cell featuring full-area HTPC deposited on both sides of the Si wafer. Noticeably, the rear-side poly-SiC<sub>x</sub>(p) hole selective contact is deposited by plasma-enhanced chemical vapor deposition (PECVD) on a KOH-etched textured surface to maximize the infrared light response (light trapping) of the bottom c-Si cell. Reaching sufficient passivation quality and hole transport properties has proven challenging on textured c-Si surfaces, limiting our previous demonstrations of perovskite/Si HTPC tandems to designs featuring a flat poly-SiC<sub>x</sub>(p) contact at the rear of the bottom cell.<sup>12</sup> Indeed, surface passivation is known to be weaker in p-type poly-Si/SiO<sub>x</sub> stack, compared with the n-type poly-Si/SiO<sub>x</sub> stack.<sup>13–22</sup> This difference has been shown to be even more dramatic on textured surfaces,<sup>21–23</sup> possibly due to the poorer passivation quality at the ⟨111⟩ surface-oriented plane (textured) compared to the ⟨100⟩ (planar).<sup>22</sup> The 28%-device presented in the current work also benefits from previous work<sup>24</sup> on low-temperature metallization screen-printing processes, which are used in the c-Si photovoltaic industry.

To assess the potential of the newly developed p-type contact, symmetric, both-sides textured samples were fabricated on p-type c-Si wafers. Textured float zone (FZ) p-type wafers (4") were used with a thickness of ~190 μm and a resistivity of ~2 Ω cm. After standard wafer cleaning, a ~1.2 nm-thick SiO<sub>x</sub> layer was grown by plasma enhanced chemical vapor deposition (PECVD). A boron-doped silicon carbide (SiC<sub>x</sub>(p)) film with a

<sup>a</sup> CSEM SA, Sustainable Energy, Jaquet-Droz 1, 2002 Neuchâtel, Switzerland.  
E-mail: andrea.ingenito@csem.ch

<sup>b</sup> Institute of Electrical and Microengineering (IEM), Photovoltaics and Thin-Film Electronics Laboratory (PV-Lab), Ecole Polytechnique Fédérale de Lausanne (EPFL), Rue de la Maladière 71b, 2002 Neuchâtel, Switzerland

† Electronic supplementary information (ESI) available: Fabrication details, device characterization, large area tandems. See DOI: <https://doi.org/10.1039/d3ya00048f>

‡ Current address: Institut Interdisciplinaire d'Innovation Technologique (3IT), Sherbrooke University, Sherbrooke, Canada.

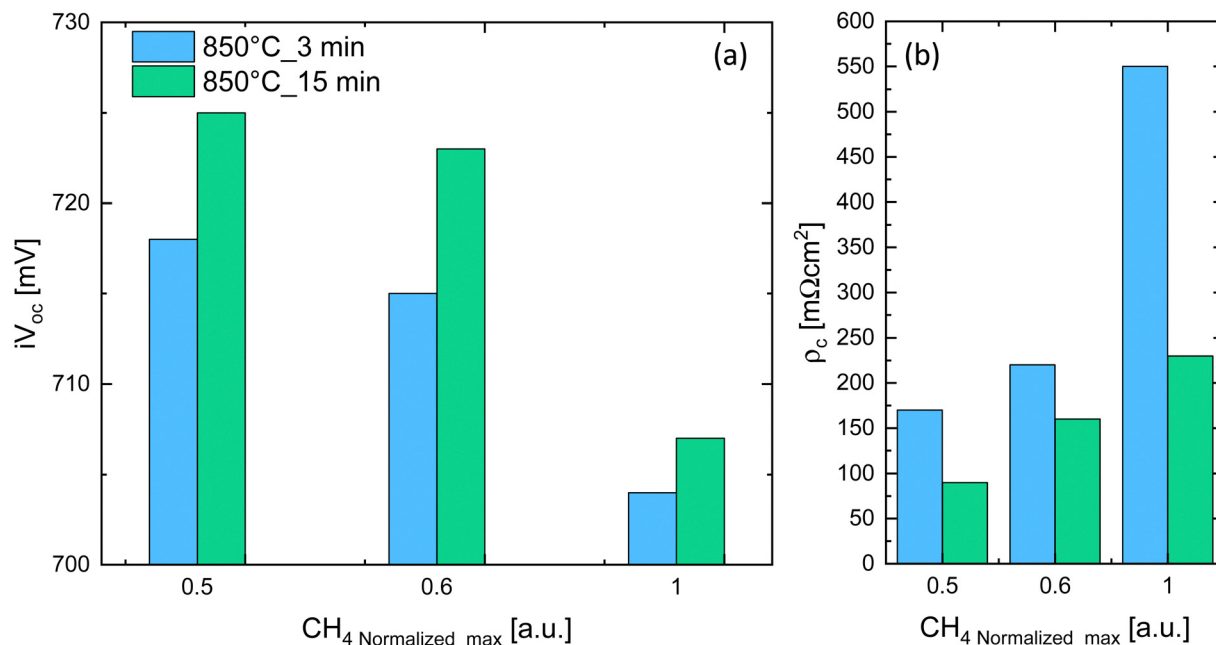


**Fig. 1** (a) Implied open circuit voltage ( $iV_{OC}$ ) and (b) specific contact resistance ( $\rho_c$ ) as a function of the CH<sub>4</sub> flow normalized to the maximum value ( $CH_4/CH_{4\max}$ ), CH<sub>4</sub> Normalized\_max. The SiC<sub>x</sub>(p) is deposited here on both sides of textured wafers.

thickness of 45 nm (on flat) was symmetrically deposited by PECVD. The samples were then annealed in a tube furnace at 850 °C, typically with a dwell time of 15 min. This treatment is required to crystallize the SiC<sub>x</sub> contact and promote the diffusion of dopants from the contact to the Si wafer. After annealing, SiN<sub>x</sub>:H was deposited by PECVD, followed by firing at 800 °C in an inline furnace for the hydrogenation of defects. After stripping of the SiN<sub>x</sub>:H in HF, ITO was deposited by sputtering through a hard metallic mask to define the contact geometry used for contact resistance ( $\rho_c$ ) measurements. Fig. 1(a) and (b) reports the implied open circuit voltage ( $iV_{OC}$ ) and the specific contact resistance ( $\rho_c$ ) measured on symmetric textured samples as a function of the CH<sub>4</sub> flow used to deposit the SiC<sub>x</sub>(p) contact by PECVD (normalized to its maximum value, CH<sub>4</sub>/CH<sub>4</sub> Normalized\_max). Excellent  $iV_{OC}$  of 725 mV and  $\rho_c$  below 90 mΩ cm<sup>2</sup> were obtained for a CH<sub>4</sub> Normalized\_max = 0.5 and for an annealing temperature of 850 °C for a dwell time of 15 min. To our knowledge these are among the best values reported so far for ap-type HTPC on a textured Si substrate.<sup>22,23</sup>

The decrease in  $iV_{OC}$  and increase in  $\rho_c$  towards higher CH<sub>4</sub> flows is explained by the higher amount of C that can disrupt the interfacial SiO<sub>x</sub> and lowers B-doping incorporation for films richer in C.<sup>25,26</sup> We hypothesize that the lower  $iV_{OC}$  and higher  $\rho_c$  for annealing dwell time of 3 min compared to 15 min (for the same normalized CH<sub>4</sub> flow) is explained by a shallower B in-diffused region into the c-Si wafer.<sup>12,14,17,27–31</sup> Rear-side textured HTPC bottom cells were processed on single-side textured FZ p-type wafers (4") of the same thickness and base resistivity as the symmetrical samples. On the rear-side, the above-optimized SiC<sub>x</sub>(p) was deposited while a SiC<sub>x</sub>(n) as reported by Ingenito *et al.*<sup>25</sup> was used for the front planar side. After stripping in HF of the SiN<sub>x</sub>:H used to hydrogenate the

contact,  $iV_{OC}$  values up to 723 mV are obtained on p-type wafers.

Taking advantage of the superior passivating properties of this new p-contact on textured c-Si wafers, PK/Si tandems were fabricated. Fig. 2(a) shows schematically the perovskite/Si HTPC device. Following the stripping of the SiN<sub>x</sub>, the ITO/Ag back electrode was created by sputtering. For the monolithic interconnection of the tandem sub-cells, a 10 nm-thin ITO recombination junction was sputtered onto the front SiC<sub>x</sub>(n) through a shadow mask. The top cell absorber had a composition of Cs<sub>0.17</sub>FA<sub>0.83</sub>Pb(I<sub>0.83</sub>Br<sub>0.17</sub>)<sub>3</sub>, corresponding to a bandgap of 1.63 eV. Interface recombination plays a significant role in perovskite solar cells, affecting both ideality factor and  $V_{OC}$ .<sup>32</sup> Similar to Al-Ashouri *et al.*,<sup>33</sup> we employ a self-assembled monolayer (SAM) made of Me-4PACz as the hole transport layer (HTL), enabling excellent interface passivation and hole selectivity. A wetting layer made of SiO<sub>x</sub> nanoparticles was added. On the Electron transport layer (ETL) side, a thin layer of LiF is thermally evaporated between the perovskite and the C<sub>60</sub> ETL. It is to be noted that the perovskite absorber was deposited on the full area of the 4" Si wafer, with each 4 cm<sup>2</sup> tandem being then defined by the deposition of the front ITO electrode through a 7-cell metal mask. A Ag paste was then screen-printed at low temperature to metallize the cell,<sup>24</sup> before depositing a LiF antireflective coating (ARC). Fig. 2(b) shows a picture of the 7 tandem cells on a 4" wafer.

The current-voltage ( $JV$ ) characteristics of the tandem cells were measured using a calibrated two-lamp solar simulator. The  $JV$  curve of the best device is displayed in Fig. 2(c). The cell was measured in the reverse (from  $V_{OC}$  to  $J_{SC}$ ) and in the forward (from  $J_{SC}$  to  $V_{OC}$ ) directions, highlighting a negligible hysteresis in these scan rate conditions (0.19 V s<sup>-1</sup>). The reverse



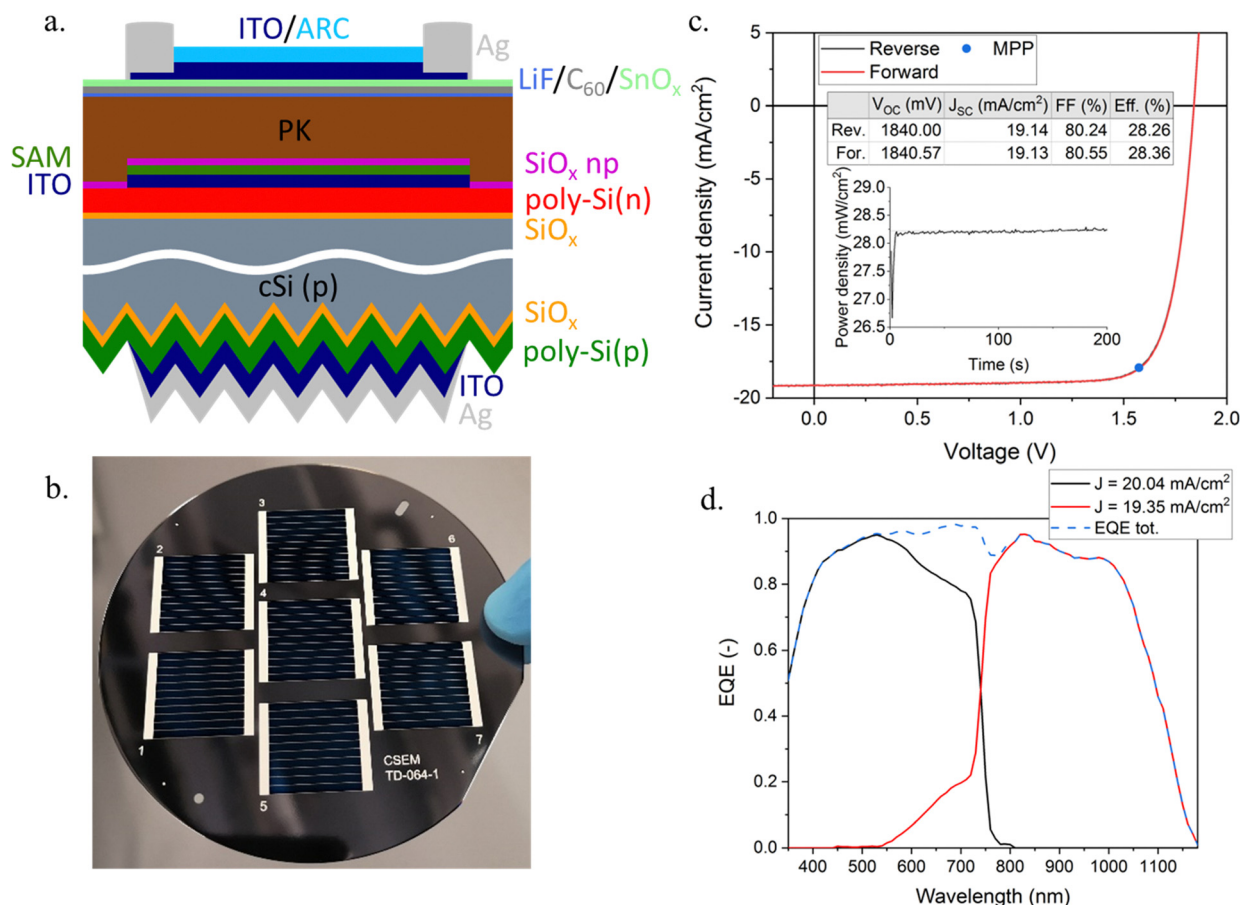


**Fig. 2** (a) Schematic view of the tandem cell stack. (b) Image of 7 tandem cells on a 4" wafer. The metallization is done by screenprinting. (c) Current–voltage (JV) characteristics of the best performing 4 cm<sup>2</sup> cell. The inset table shows the JV parameters of the reverse ( $V_{OC} \rightarrow J_{SC}$ , black) and forward ( $J_{SC} \rightarrow V_{OC}$ , red) scans. The inset graph provides the maximum power point (MPP) tracking over 200 s, showing a steady-state efficiency of 28.25%. (d) External quantum efficiency (EQE) spectra of the top perovskite (black) and bottom Si HTPC (red) sub-cells. The blue dashed line shows the sum of the two.

JV measurement yields a  $V_{OC}$  of 1840 mV, a  $J_{SC}$  of 19.14 mA cm<sup>-2</sup> and a Fill factor (FF) of 80.24%, resulting in a PCE of 28.26%, a value on par with record values reported with 4 cm<sup>2</sup> perovskite/Si cells.<sup>34</sup> This result is confirmed by a maximum power point tracking (MPP) over 200 s, which converges to a maximum power density of 28.25 mW cm<sup>-2</sup> (average power over the last 60 s of tracking), as can be seen in the inset of Fig. 2(c). Fig. 2(d) shows the EQE measurement of the two sub-cells. From the integrated current density, one can infer that, with a top cell current of 20.04 mA cm<sup>-2</sup> and a bottom cell current of 19.35 mA cm<sup>-2</sup>, the tandem device power output is limited by the bottom cell current, which may hence explain the high FF of the device<sup>35</sup> (>80%). The monochromatic light spot of the EQE measurement is focused between the silver lines of the front metallization, thus excluding shadow losses and hence explaining the discrepancy with the  $J_{sc}$  from the JV curve. Fig. S1 of the ESI† shows the distribution of the JV parameters across the 4" Si wafer, demonstrating the good uniformity over a large area.

Thanks to the scalability of the different techniques involved – and notably of the metallization, we have successfully upscaled the process for perovskite/silicon tandem devices to a 4" pseudo-square with an active area of 57.4 cm<sup>2</sup>. The device exhibited a PCE

of 22.51%. The perovskite layer and the front grid metallization were deposited using the same deposition approach as for the small area devices. These results demonstrate the potential for further optimization and scaling of perovskite/silicon tandem devices. This result is summarized in Fig. S2 (ESI†).

To conclude, we report here a perovskite/Si tandem solar cell based on a both-side passivating contact bottom cell architecture with a poly-Si(p) passivating contact deposited on the textured rear-side of the Si cell. This device reaches a power conversion efficiency of 28.25% on an active area of 4 cm<sup>2</sup>, in part thanks to a FF above 80%. These results demonstrate that Si cells based on HTPC, a category of contacts that is gaining traction on the PV market, can be combined with a perovskite top cell to reach efficiencies comparable to those reached with perovskite/Si tandems, and are also scalable to larger active area than those typically reported in the literature (1 cm<sup>2</sup>).

## Author contributions

A. W. and A. I.: conceptualization, data curation, formal analysis, investigation, methodology, validation, visualization,



writing – original draft; P.W.: investigation and resources; B. A. K., S.-J. M. J. J. D.L., C. A. and A. D.: conceptualization, investigation, methodology, validation; S. N and Q. J.: funding acquisition, project administration and supervision; C. B.: supervision. All: writing – review and editing.

## Conflicts of interest

There are no conflicts to declare.

## Acknowledgements

Part of the work presented here has received funding from the European Union's Horizon 2020 research and innovation program under Grant Agreement No. 861985 (project PeroCUBE), and from the Swiss National Science Foundation (SNSF) in the framework of the project PAPET (200021\_197006).

## Notes and references

- 1 NREL, Best Res. Effic. Chart.
- 2 X. Y. Chin, D. Türkay, J. Steele, S. Tabean, S. Eswara, M. Mensi, P. Fiala, C. M. Wolff, A. Paracchino, K. Artuk, D. Jacobs, Q. Guesnay, F. Sahli, G. Andreatta, M. Boccard, Q. Jeangros and C. Ballif, Interface passivation for 31.25%-efficient perovskite/silicon tandem solar cells, *Science*, 2023, 59–63, in print.
- 3 S. Mariotti, E. Köhnen, F. Scheler, K. Sveinbjörnsson, L. Zimmermann, M. Piot, F. Yang, B. Li, J. Warby, A. Musiienko, D. Menzel, F. Lang, S. Kefßler, I. Levine, D. Mantione, A. Al-Ashouri, M. S. Härtel, K. Xu, A. Cruz, J. Kurpiers, P. Wagner, H. Köbler, J. Li, A. Magomedov, D. Mecerreyes, E. Unger, A. Abate, M. Stollerfoht, B. Stannowski, R. Schlattmann, L. Korte and S. Albrecht, Interface engineering for high-performance, triple-halide perovskite-silicon tandem solar cells, *Science*, 2023, **381**, 63–69.
- 4 F. Fu, J. Li, T. C. Yang, H. Liang, A. Faes, Q. Jeangros, C. Ballif and Y. Hou, Monolithic Perovskite-Silicon Tandem Solar Cells: From the Lab to Fab?, *Adv. Mater.*, 2022, **34**, 2106540.
- 5 A. Al-Ashouri, E. Köhnen, B. Li, A. Magomedov, H. Hempel, P. Caprioglio, J. A. Márquez, A. B. M. Vilches, E. Kasparavicius, J. A. Smith, N. Phung, D. Menzel, M. Grischek, L. Kegelmann, D. Skroblin, C. Gollwitzer, T. Malinauskas, M. Jošt, G. Matič, B. Rech, R. Schlattmann, M. Topič, L. Korte, A. Abate, B. Stannowski, D. Neher, M. Stollerfoht, T. Unold, V. Getautis and S. Albrecht, Monolithic perovskite/silicon tandem solar cell with >29% efficiency by enhanced hole extraction, *Science*, 2020, **370**, 1300–1309.
- 6 Cell, KAUST claims 33.7% efficiency for perovskite/silicon tandem solar, <https://www.pv-magazine.com/2023/05/30/kaust-claims-33-7-efficiency-for-perovskite-silicon-tandem-solar-cell/>.
- 7 K. Sveinbjörnsson, B. Li, S. Mariotti, E. Jarzembowski, L. Kegelmann, A. Wirtz, F. Frühauf, A. Weihrauch, R. Niemann, L. Korte, F. Fertig, J. W. Müller and S. Albrecht, Monolithic Perovskite/Silicon Tandem Solar Cell with 28.7% Efficiency Using Industrial Silicon Bottom Cells, *ACS Energy Lett.*, 2022, **7**, 2654–2656.
- 8 S. Mariotti, K. Jäger, M. Diederich, M. S. Härtel, B. Li, K. Sveinbjörnsson, S. Kajari-Schröder, R. Peibst, S. Albrecht, L. Korte and T. Wietler, Monolithic Perovskite/Silicon Tandem Solar Cells Fabricated Using Industrial p-Type Polycrystalline Silicon on Oxide/Passivated Emitter and Rear Cell Silicon Bottom Cell Technology, *Sol. RRL*, 2022, **6**, 2101066.
- 9 VDMA, International Technology Roadmap for Photovoltaic, 2022, vol. 13th Edition.
- 10 Y. Wu, P. Zheng, J. Peng, M. Xu, Y. Chen, S. Surve, T. Lu, A. D. Bui, N. Li, W. Liang, L. Duan, B. Li, H. Shen, T. Duong, J. Yang, X. Zhang, Y. Liu, H. Jin, Q. Chen, T. White, K. Catchpole, H. Zhou and K. Weber, 27.6% Perovskite/c-Si Tandem Solar Cells Using Industrial Fabricated TOPCon Device, *Adv. Energy Mater.*, 2022, **12**, 2200821.
- 11 Z. Ying, Z. Yang, J. Zheng, H. Wei, L. Chen, C. Xiao, J. Sun, C. Shou, G. Qin, J. Sheng, Y. Zeng, B. Yan, X. Yang and J. Ye, Monolithic perovskite/black-silicon tandems based on tunnel oxide passivated contacts, *Joule*, 2022, **6**, 1–18.
- 12 G. Nogay, F. Sahli, J. Werner, R. Monnard, M. Boccard, M. Despeisse, F.-J. Haug, Q. Jeangros, A. Ingenito and C. Ballif, 25.1%-Efficient monolithic perovskite/silicon tandem solar cell based on a p-type monocrystalline textured silicon wafer and high-temperature passivating contacts, *ACS Energy Lett.*, 2019, **4**, 844–845.
- 13 U. Römer, R. Peibst, T. Ohrdes, B. Lim, J. Krügener, E. Bugiel, T. Wietler and R. Brendel, Recombination behavior and contact resistance of n+ and p+ poly-crystalline Si/mono-crystalline Si junctions, *Sol. Energy Mater. Sol. Cells*, 2014, **131**, 85–91.
- 14 M. Lozac'h, S. Nunomura, H. Sai and K. Matsubara, Passivation property of ultrathin SiOx:H/a-Si:H stack layers for solar cell applications, *Sol. Energy Mater. Sol. Cells*, 2018, **185**, 8–15.
- 15 F. Feldmann, R. Müller, C. Reichel and M. Hermle, Ion implantation into amorphous Si layers to form carrier-selective contacts for Si solar cells, *Phys. Status Solidi RRL*, 2014, **08**, 767–770.
- 16 F. Feldmann, M. Simon, M. Bivour, C. Reichel, M. Hermle and S. W. Glunz, Carrier-selective contacts for Si solar cells, *Appl. Phys. Lett.*, 2014, **104**, 181105.
- 17 U. Römer, R. Peibst, T. Ohrdes, B. Lim, J. Krügener, T. Wietler and R. Brendel, Ion implantation for poly-Si passivated back-junction back-contacted solar cells, *IEEE J. Photovoltaics*, 2015, **5**, 507–514.
- 18 D. L. Young, W. Nemeth, V. LaSalvia, R. Reedy, S. Essig, N. Bateman and P. Stradins, Interdigitated Back Passivated Contact (IBPC) Solar Cells Formed by Ion Implantation, *IEEE J. Photovoltaics*, 2016, **6**, 41–47.





- 19 C. Reichel, F. Feldmann, R. Müller, R. C. Reedy, B. G. Lee, D. L. Young, P. Stradins, M. Hermle and S. W. Glunz, Tunnel oxide passivated contacts formed by ion implantation for applications in silicon solar cells, *J. Appl. Phys.*, 2015, **118**, 205701.
- 20 D. Yan, A. Cuevas, J. Bullock, Y. Wan and C. Samundsett, Phosphorus-diffused polysilicon contacts for solar cells, *Sol. Energy Mater. Sol. Cells*, 2015, **142**, 75–82.
- 21 A. Ingenito, G. Nogay, J. Stuckelberger, P. Wyss, L. Gnocchi, C. Allebe, J. Horzel, M. Despeisse, F.-J. Haug, P. Loper and C. Ballif, Phosphorous-Doped Silicon Carbide as Front-Side Full-Area Passivating Contact for Double-Side Contacted c-Si Solar Cells, *IEEE J. Photovoltaics*, 2019, **9**, 346–354.
- 22 Y. Larionova, M. Turcu, S. Reiter, R. Brendel, D. Tetzlaff, J. Krügener, T. Wietler, U. Höhne, J.-D. Kähler and R. Peibst, On the recombination behavior of p+ -type polysilicon on oxide junctions deposited by different methods on textured and planar surfaces, *Phys. Status Solidi*, 2017, 1700058.
- 23 M. Stodolny, K. Tool, B. Geerligs, J. Löffler, A. Weeber, Y. Wu, J. Anker, X. Lu, J. Liu, P. Bronsveld, A. Mewe, G. Janssen and G. Coletti, PolySi Based Passivating Contacts Enabling Industrial Silicon Solar Cell Efficiencies up to 24%, *Conf. Rec. IEEE Photovolt. Spec. Conf.*, 2019, 1456–1459.
- 24 B. A. Kamino, B. Paviet-Salomon, S.-J. Moon, N. Badel, J. Levrat, G. Christmann, A. Walter, A. Faes, L. Ding, J. J. Diaz Leon, A. Paracchino, M. Despeisse, C. Ballif and S. Nicolay, Low-Temperature Screen-Printed Metallization for the Scale-Up of Two-Terminal Perovskite-Silicon Tandems, *ACS Appl. Energy Mater.*, 2019, **2**, 3815–3821.
- 25 A. Ingenito, G. Nogay, J. A. Stuckelberger, P. Wyss, J. Horzel, C. Allebé, M. Despeisse, F.-J. Haug, P. Löper and C. Ballif, in *33rd European Photovoltaic Solar Energy Conference and Exhibition (EU PVSEC)*, Amsterdam, 2017.
- 26 A. Ingenito, G. Nogay, Q. Jeangros, E. Rucavado, C. Allebé, S. Eswara, N. Valle, T. Wirtz, J. Horzel and T. Koida, A passivating contact for silicon solar cells formed during a single firing thermal annealing, *Nat. Energy*, 2018, **3**, 800.
- 27 G. Nogay, J. Stuckelberger, P. Wyss, E. Rucavado, C. Allebé, T. Koida, M. Morales-masis, M. Despeisse, F. Haug, P. Löper and C. Ballif, Interplay of annealing temperature and doping in hole selective rear contacts based on silicon-rich silicon-carbide thin films, *Sol. Energy Mater. Sol. Cells*, 2017, **173**, 18–24.
- 28 M. Lehmann, N. Valle, J. Horzel, A. Pshenova, P. Wyss, M. Döbeli, M. Despeisse, S. Eswara, T. Wirtz, Q. Jeangros, A. Hessler-wyser, F. Haug, A. Ingenito, C. Ballif, E. Polytechnique, F. De Lausanne, M. Imt, T. Film and R. D. La Maladière, Analysis of hydrogen distribution and migration in fired passivating contacts, *Sol. Energy Mater. Sol. Cells*, 2019, **200**, 110018.
- 29 G. Yang, A. Ingenito, N. Van Hameren, O. Isabella and M. Zeman, Design and application of ion-implanted polySi passivating contacts for interdigitated back contact c-Si solar cells, *Appl. Phys. Lett.*, 2016, **108**, 033903.
- 30 H. Steinkemper, F. Feldmann, M. Bivour and M. Hermle, Theoretical Investigation of Carrier-selective Contacts Featuring Tunnel Oxides by Means of Numerical Device Simulation, *Energy Procedia*, 2015, **77**, 195–201.
- 31 P. Procel, P. Löper, F. Crupi, C. Ballif and A. Ingenito, Numerical simulations of hole carrier selective contacts in p-type c-Si solar cells, *Sol. Energy Mater. Sol. Cells*, 2019, **200**, 109937.
- 32 P. Caprioglio, C. M. Wolff, O. J. Sandberg, A. Armin, B. Rech, S. Albrecht, D. Neher and M. Stollerfoht, On the Origin of the Ideality Factor in Perovskite Solar Cells, *Adv. Energy Mater.*, 2020, **10**, 1–9.
- 33 A. Al-Ashouri, E. Köhnen, B. Li, A. Magomedov, H. Hempel, P. Caprioglio, J. A. Márquez, A. B. Morales Vilches, E. Kasparavicius, J. A. Smith, N. Phung, D. Menzel, M. Grischek, L. Kegelmann, D. Skroblin, C. Gollwitzer, T. Malinauskas, M. Jošt, G. Matič, B. Rech, R. Schlatmann, M. Topič, L. Korte, A. Abate, B. Stannowski, D. Neher, M. Stollerfoht, T. Unold, V. Getautis and S. Albrecht, Monolithic perovskite/silicon tandem solar cell with >29% efficiency by enhanced hole extraction, *Science*, 2020, **370**, 1300–1309.
- 34 D. Kirk, *tandemPV Workshop*, Freiburg, 2022.
- 35 M. Boccard and C. Ballif, Influence of the Subcell Properties on the Fill Factor of Two-Terminal Perovskite-Silicon Tandem Solar Cells, *ACS Energy Lett.*, 2020, **5**, 1077–1082.

